

Supplementary Materials

One-Dimensional Perovskite with Ferroelectric and Switchable Nonlinear

Optical Properties: [azetidinium]CdCl₃

Magdalena Rok^a, Bartosz Zarychta^b, Andrzej Bil^a, Joanna Trojan-Piegza^a, Anna Piecha-Bisiolek^a, Jan K. Zaręba^c, Wojciech Medycki^d, Ryszard Jakubas^a

^aFaculty of Chemistry, University of Wrocław, 14 F. Joliot – Curie, 50-383 Wrocław, Poland

^bFaculty of Chemistry, University of Opole, Opole PL-45052, Poland

^cAdvanced Materials Engineering and Modelling Group, Faculty of Chemistry, Wrocław University of Science and Technology, Wybrzeże Wyspiańskiego 27, 50-370 Wrocław, Poland

^dInstitute of Molecular Physics, Polish Academy of Sciences, Smoluchowskiego 17, 60-179 Poznań, Poland

* e-mail: magdalena.rok@chem.uni.wroc.pl

CAPTIONS OF FIGURES

- Figure S1.** The simultaneous TGA/DSC analyses for **AZECdCl₃** (sample mass $m = 17.6500$ mg, 5K/min. 6
- Figure S2.** SHG spectra collected in the heating cycle (133-217 K) for **AZECdCl₃**, excitation 800 nm. 7
- Figure S3.** SHG spectra collected in the cooling cycle (214-130K K) for **AZECdCl₃**, excitation 800 nm... 7
- Figure S4.** The temperature dependence of the dielectric permittivity, ϵ' and ϵ'' , obtained on cooling run for single crystals cut perpendicular to the a and b) *a*-axis ($S = 4$ mm², $d = 1.1$ mm), c and d) *b*-axis ($S = 16$ mm², $d = 0.82$ mm). 9
- Figure S5.** The temperature dependence of the dielectric permittivity, a) ϵ' and b) ϵ'' , obtained on cooling run for single crystals cut perpendicular to the *c*-axis. The 'y' is in *log*-scale..... 10
- Figure S6.** The frequency dependence of the dielectric permittivity, (a) ϵ' and (b) ϵ'' , obtained on cooling run for single crystals cut perpendicular to the *c*-axis. Data was presented for chosen temperatures from II phase. (c) and (d) Data was presented for chosen temperatures from III phase. e) The temperature dependence of the macroscopic dielectric relaxation time presented in Arrhenius relation. Red points present the relaxation time from NMR measurement, black from dielectric relaxation..... 11
- Figure S7.** a) P-E vs. frequency and b) drive voltage for 1Hz. Both diagrams were measured at 170K.12
- Figure S8.** Graphical representation of the disordered phase III (*Cmc2₁*) and representations A and B of the ordered phase obtained by fixing the position of the azetidinium cation. 14
- Figure S9.** Temperature dependence of second moment of ¹HNMR line of **AZECdCl₃**. 16
- Figure S10.** Temperature dependence of excitation spectra monitored at 370 nm (a), 410 nm (b) and 620 nm (c)..... 17
- Figure S11.** Normalized temperature-dependent emission spectra excited with (a) 281 nm and (b) 291 nm..... 18
- Figure S12.** Temperature dependence of the integrated emission intensity (brown spheres) and FWHM (blue spheres) for emission excited with 281 nm (top) and 291 nm (bottom). 19
- Figure S13.** Gaussian deconvolution of 15K photoluminescence. 20

Figure S14. Temperature dependence of indicated emission decays.	21
Figure S15. The X-ray diffraction pattern at 298 K of AZECdCl₃ (blue) and calculated from crystal structure (pink).....	22

CAPTIONS OF TABLES

Table S1. Experimental details for (AZECdCl₃)	3
Table S2. Selected geometric parameters (Å, °) for (AZECdCl₃)	4
Table S3. Hydrogen-bond geometry (Å, °) for (AZECdCl₃)	5
Table S4. Thermodynamic parameters of the phase transition for AZECdCl₃ in the condensed state measured upon heating cycle.....	8
Table S5. Spontaneous polarization components [$\mu\text{C}/\text{cm}^2$] for the ordered model of the non-centrosymmetric phase calculated within Berry phase approach using LDA functional. For ‘a’ axis a polarization indetermination quantum is a multiple of 14.90 $\mu\text{C}/\text{cm}^2$. For ‘c’ axis a polarization indetermination quantum is a multiple of 13.37 $\mu\text{C}/\text{cm}^2$	13
Table S6. Spontaneous polarization components [$\mu\text{C}/\text{cm}^2$] for the ordered models of the non-centrosymmetric phase calculated within Berry phase approach using PBA functional.....	13
Table S7. Temperature dependence of average lifetimes of indicated emissions.....	21

Table S1. Experimental details for (AZECDCl₃)

For all structures: $M_r = 276.85$, $Z = 4$. Experiments were carried out with Mo $K\alpha$ radiation using a Xcalibur, Sapphire2, large Be window. Absorption was corrected for by multi-scan methods, *CrysAlis RED*, Oxford Diffraction Ltd., Version 1.171.33.57 (release 26-01-2010 CrysAlis171 .NET) (compiled Jan 26 2010,14:36:55) Empirical absorption correction using spherical harmonics, implemented in SCALE3 ABSPACK scaling algorithm. H-atom parameters were constrained.

	(II)	(III)	(IV)
Crystal data			
Chemical formula	(AZECDCl ₃), (C ₃ H ₈ N)CdCl ₃		
Crystal system, space group	Orthorhombic, <i>Cmcm</i>	Orthorhombic, <i>Cmc2₁</i>	Orthorhombic, <i>Pbnm</i>
Temperature (K)	220	185	100
a, b, c (Å)	7.4277 (5), 16.1607 (10), 6.6625 (5)	7.4202 (3), 16.1485 (5), 6.6581 (2)	8.0355 (3), 14.8293 (5), 6.6254 (2)
V (Å ³)	799.75 (9)	797.81 (5)	789.49 (5)
μ (mm ⁻¹)	3.64	3.65	3.69
Crystal size (mm)	0.35 × 0.20 × 0.18		
Data collection			
T_{\min}, T_{\max}	0.547, 1.000	0.588, 1.000	0.453, 1.000
No. of measured, independent and observed [$I > 2\sigma(I)$] reflections	1812, 445, 426	4224, 837, 835	4047, 835, 817
R_{int}	0.046	0.064	0.047
$(\sin \theta/\lambda)_{\text{max}}$ (Å ⁻¹)	0.617	0.616	0.617
Refinement			
$R[F^2 > 2\sigma(F^2)],$ $wR(F^2), S$	0.039, 0.099, 1.08	0.028, 0.071, 1.03	0.038, 0.108, 1.11
No. of reflections	445	837	835
No. of parameters	40	51	47
No. of restraints	30	31	0
$\Delta\rho_{\text{max}}, \Delta\rho_{\text{min}}$ (e Å ⁻³)	1.04, -0.70	0.70, -0.55	1.06, -0.87

Computer programs: *CrysAlis CCD*, Oxford Diffraction, 2007, *CrysAlis RED*, *SHELXL2014/7* (Sheldrick, 2014), *Mercury* 2020.3.0 (Macrae *et al.*, 2020).

Table S2. Selected geometric parameters (Å, °) for (AZECdCl₃)

(II)			
Cd1—Cl1 ⁱ	2.6117 (8)	N1—C2A ^{vi}	1.481 (13)
Cd1—Cl1 ⁱⁱ	2.6117 (8)	N1—C2B	1.48 (2)
Cd1—Cl1	2.6117 (8)	C2A—N1 ^{vi}	1.481 (13)
Cd1—Cl1 ⁱⁱⁱ	2.6117 (8)	C2A—C3 ^{vii}	1.49 (3)
Cd1—Cl2 ⁱ	2.6641 (10)	C2A—C3	1.49 (3)
Cd1—Cl2	2.6642 (10)	C2B—C3 ^{vii}	1.49 (2)
Cd1—Cd1 ^{iv}	3.3312 (3)	C2B—C3	1.49 (2)
Cd1—Cd1 ^v	3.3312 (3)	C2B—C2B ^{vi}	1.67 (3)
Cl1—Cd1 ^{iv}	2.6117 (8)	C3—C2B ^{vi}	1.49 (2)
Cl2—Cd1 ^{iv}	2.6642 (10)	C3—C2A ^{vi}	1.49 (3)
(III)			
Cd1—Cl1 ^{viii}	2.605 (2)	Cl1—Cd1 ^{iv}	2.620 (2)
Cd1—Cl1	2.605 (2)	Cl2—Cd1 ^{iv}	2.646 (2)
Cd1—Cl1 ^v	2.620 (2)	N1—C2	1.424 (15)
Cd1—Cl1 ⁱⁱⁱ	2.620 (2)	N1—C2'	1.519 (15)
Cd1—Cl2 ^v	2.646 (2)	C2—C3	1.44 (2)
Cd1—Cl2	2.680 (2)	C2—C3 ^{ix}	1.44 (2)
Cd1—Cd1 ^v	3.3304 (1)	C3—C2'	1.494 (18)
Cd1—Cd1 ^{iv}	3.3304 (1)	C2'—C3 ^{ix}	1.494 (18)
(IV)			
Cd1—Cl1 ⁱⁱ	2.5842 (8)	Cl1—Cd1 ^{iv}	2.6679 (8)
Cd1—Cl1'	2.5843 (8)	Cl1'—Cd1 ^v	2.5843 (8)
Cd1—Cl2 ⁱ	2.6432 (8)	Cl2—Cd1 ^{iv}	2.6432 (8)
Cd1—Cl2	2.6432 (8)	N1—C2	1.503 (6)
Cd1—Cl1	2.6679 (8)	N1—C2 ^{vi}	1.503 (6)
Cd1—Cl1 ⁱ	2.6679 (8)	C2—C3	1.513 (6)
Cd1—Cd1 ^v	3.3127 (1)	C3—C2 ^{vi}	1.513 (6)
Cd1—Cd1 ^{iv}	3.3127 (1)		
(II)			
Cl1 ⁱ —Cd1—Cl1 ⁱⁱ	93.09 (4)	Cl1—Cd1—Cl2 ⁱ	97.36 (2)
Cl1 ⁱ —Cd1—Cl1	180.0	Cl1 ⁱⁱⁱ —Cd1—Cl2 ⁱ	82.64 (2)
Cl1 ⁱⁱ —Cd1—Cl1	86.91 (4)	Cl1 ⁱ —Cd1—Cl2	97.36 (2)
Cl1 ⁱ —Cd1—Cl1 ⁱⁱⁱ	86.91 (4)	Cl1 ⁱⁱ —Cd1—Cl2	82.64 (2)
Cl1 ⁱⁱ —Cd1—Cl1 ⁱⁱⁱ	180.0	Cl1—Cd1—Cl2	82.64 (2)
Cl1—Cd1—Cl1 ⁱⁱⁱ	93.09 (4)	Cl1 ⁱⁱⁱ —Cd1—Cl2	97.36 (2)
Cl1 ⁱ —Cd1—Cl2 ⁱ	82.64 (2)	Cl2 ⁱ —Cd1—Cl2	180.0
Cl1 ⁱⁱ —Cd1—Cl2 ⁱ	97.36 (2)	Cd1 ^{iv} —Cd1—Cd1 ^v	180.0
(III)			
Cl1 ^{viii} —Cd1—Cl1	87.38 (8)	Cl1 ^v —Cd1—Cl2 ^v	82.77 (7)
Cl1 ^{viii} —Cd1—Cl1 ^v	92.91 (4)	Cl1 ⁱⁱⁱ —Cd1—Cl2 ^v	82.77 (7)
Cl1—Cd1—Cl1 ^v	177.87 (5)	Cl1 ^{viii} —Cd1—Cl2	82.43 (7)
Cl1 ^{viii} —Cd1—Cl1 ⁱⁱⁱ	177.87 (5)	Cl1—Cd1—Cl2	82.43 (7)
Cl1—Cd1—Cl1 ⁱⁱⁱ	92.91 (4)	Cl1 ^v —Cd1—Cl2	95.51 (5)
Cl1 ^v —Cd1—Cl1 ⁱⁱⁱ	86.72 (9)	Cl1 ⁱⁱⁱ —Cd1—Cl2	95.51 (5)
Cl1 ^{viii} —Cd1—Cl2 ^v	99.27 (5)	Cl2 ^v —Cd1—Cl2	177.63 (11)
Cl1—Cd1—Cl2 ^v	99.27 (5)	Cd1 ^v —Cd1—Cd1 ^{iv}	176.74 (4)
(IV)			
Cl1 ⁱⁱ —Cd1—Cl1'	180.0	Cl2 ⁱ —Cd1—Cl1	96.36 (3)

C11 ⁱⁱ —Cd1—Cl2 ⁱ	96.29 (3)	Cl2—Cd1—Cl1	83.64 (3)
C11 ⁱ —Cd1—Cl2 ⁱ	83.71 (3)	C11 ⁱⁱ —Cd1—Cl1 ⁱ	93.69 (3)
C11 ⁱⁱ —Cd1—Cl2	83.71 (3)	C11 ⁱ —Cd1—Cl1 ⁱ	86.31 (3)
C11 ⁱ —Cd1—Cl2	96.29 (3)	Cl2 ⁱ —Cd1—Cl1 ⁱ	83.64 (3)
Cl2 ⁱ —Cd1—Cl2	180.0	Cl2—Cd1—Cl1 ⁱ	96.36 (3)
C11 ⁱⁱ —Cd1—Cl1	86.31 (3)	Cl1—Cd1—Cl1 ⁱ	180.0
C11 ⁱ —Cd1—Cl1	93.69 (3)	Cd1 ^v —Cd1—Cd1 ^{iv}	180.0

Symmetry code(s): (i) $-x, -y+1, -z+1$; (ii) $-x, y, -z+3/2$; (iii) $x, -y+1, z-1/2$; (iv) $-x, -y+1, z+1/2$; (v) $-x, -y+1, z-1/2$; (vi) $x, y, -z+3/2$; (vii) $-x+1, y, -z+3/2$; (viii) $-x, y, z$; (ix) $-x+1, y, z$.

Table S3. Hydrogen-bond geometry (Å, °) for (AZECdCl₃)

<i>D</i> —H··· <i>A</i>	<i>D</i> —H (Å)	H··· <i>A</i> (Å)	<i>D</i> ··· <i>A</i> (Å)	<i>D</i> —H··· <i>A</i> (°)
(II)				
N1—H1A···Cl1	0.90	2.60	3.374 (10)	144.9
N1—H1B···Cl1 ⁱ	0.90	2.60	3.374 (10)	144.9
C2A—H2BC···Cl1 ⁱⁱ	0.96	2.80	3.57 (2)	138.5
C2B—H2BC···Cl1 ⁱⁱ	0.96	2.80	3.612 (14)	142.7
C2A—H2BD···Cl1 ⁱⁱⁱ	0.96	2.80	3.57 (2)	138.5
C2B—H2BD···Cl1 ⁱⁱⁱ	0.96	2.80	3.612 (14)	142.7
C3—H3A···Cl1 ^{iv}	0.96	2.93	3.85 (3)	162.0
(III)				
N1—H1A···Cl1	0.89	2.62	3.389 (9)	145.3
N1—H1B···Cl1 ^v	0.89	2.62	3.389 (9)	145.3
C2—H2A···Cl1 ^{vi}	0.96	2.90	3.566 (10)	127.8
C3—H3B···Cl1 ^{vii}	0.96	2.96	3.901 (14)	165.7
C2'—H2'A···Cl1 ^{viii}	0.96	2.95	3.637 (9)	129.2
C2'—H2'B···Cl1 ^{ix}	0.96	2.75	3.637 (9)	153.6
(IV)				
N1—H1B···Cl2 ^x	0.89	2.32	3.159 (5)	156.5
N1—H1A···Cl1	0.89	2.45	3.283 (5)	156.8
C2—H2B···Cl1 [']	0.97	2.70	3.648 (4)	164.4
C3—H3B···Cl1 ^{vii}	0.97	2.88	3.734 (5)	147.4
C3—H3B···Cl1 ^{xi}	0.97	2.87	3.620 (5)	135.2
C3—H3A···Cl2	0.97	2.88	3.849 (6)	173.9

Symmetry code(s): (i) $-x+1, y, -z+3/2$; (ii) $-x+1, -y+1, -z+1$; (iii) $x, -y+1, z-1/2$; (iv) $-x+1/2, y-1/2, -z+3/2$; (v) $-x+1, y, z$; (vi) $-x+1, -y+1, z-1/2$; (vii) $-x+1/2, y-1/2, z$; (viii) $x, -y+1, z+1/2$; (ix) $-x+1, -y+1, z+1/2$; (x) $x+1, y, z$; (xi) $x+1/2, -y+1/2, -z+1$.

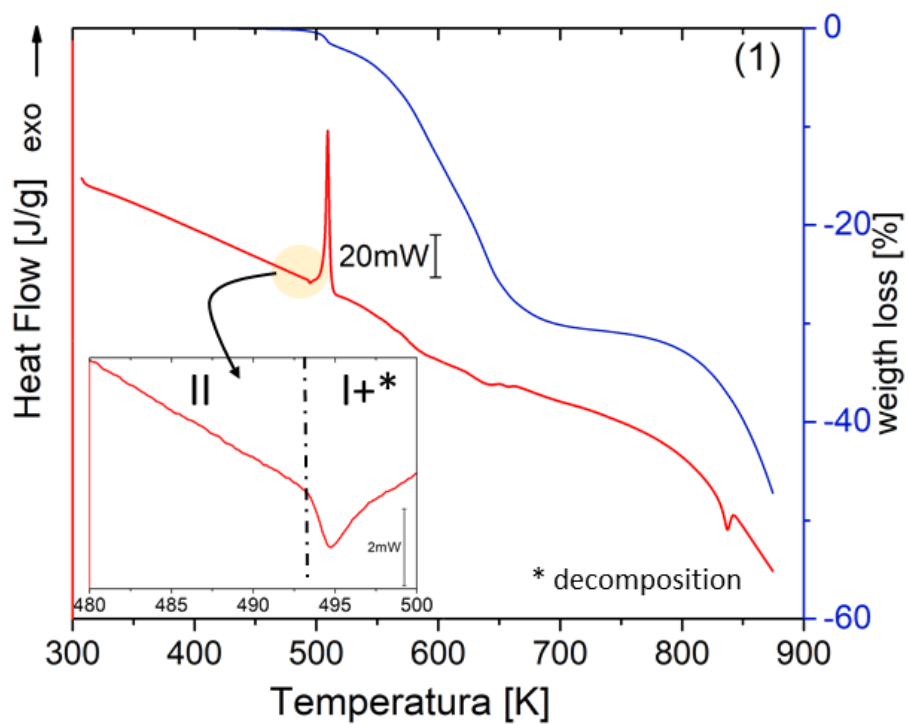


Figure S1. The simultaneous TGA/DSC analyses for AZECdCl₃ (sample mass $m = 17.6500$ mg, 5K/min).

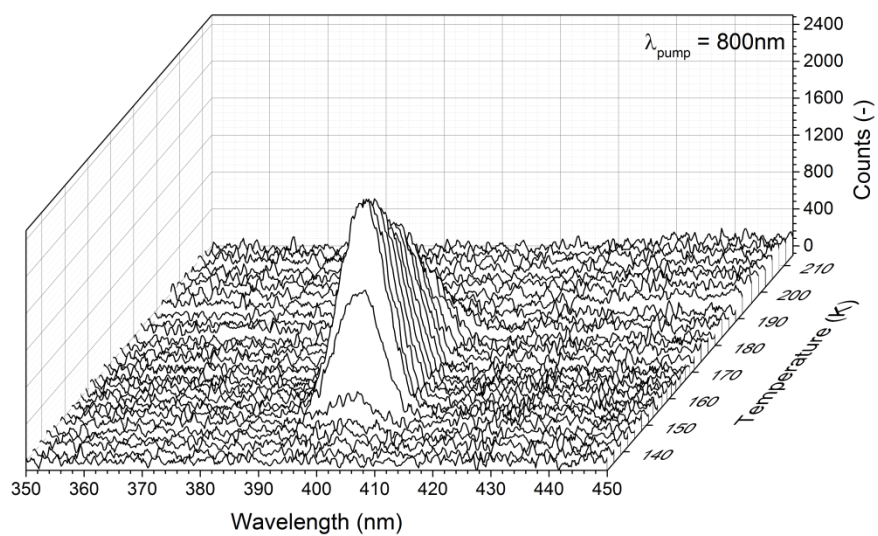


Figure S2. SHG spectra collected in the heating cycle (133-217 K) for AZECdCl_3 , excitation 800 nm.

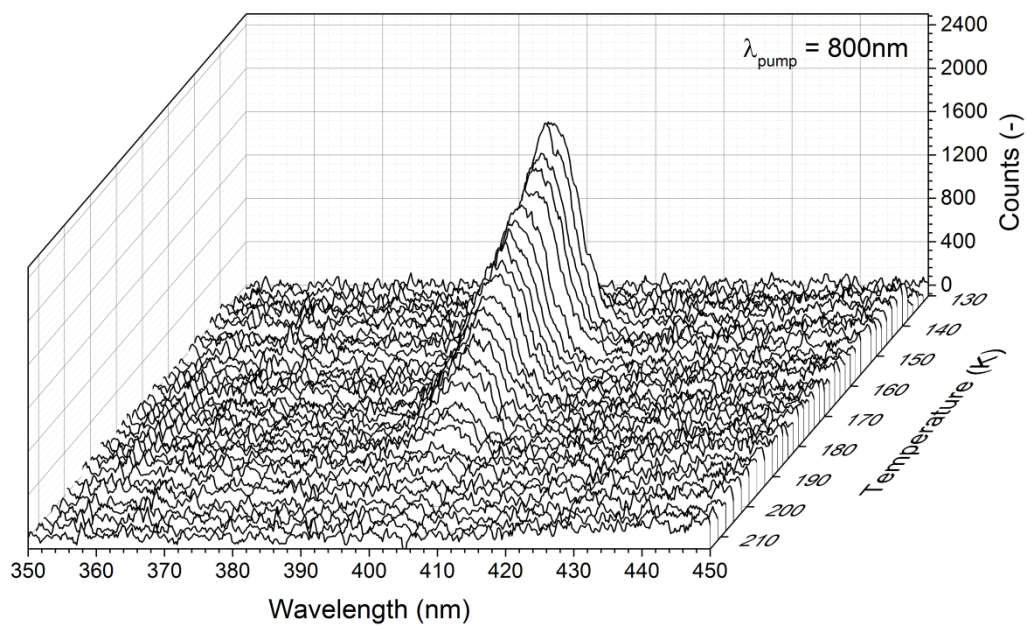


Figure S3. SHG spectra collected in the cooling cycle (214-130K K) for AZECdCl_3 , excitation 800 nm

Table S4. Thermodynamic parameters of the phase transition for **AZECdCl₃** in the condensed state measured upon heating cycle.

PT	IV→III	III→II	II→I
M [g/mol]		276.85	
T [K]	167	202	495
ΔH [J·g ⁻¹]	7.71		3.21
ΔH [J·mol ⁻¹]	2134.5		888.7
ΔS [J·mol ⁻¹ ·K ⁻¹]	12.8		1.8
N	4.7		1.2

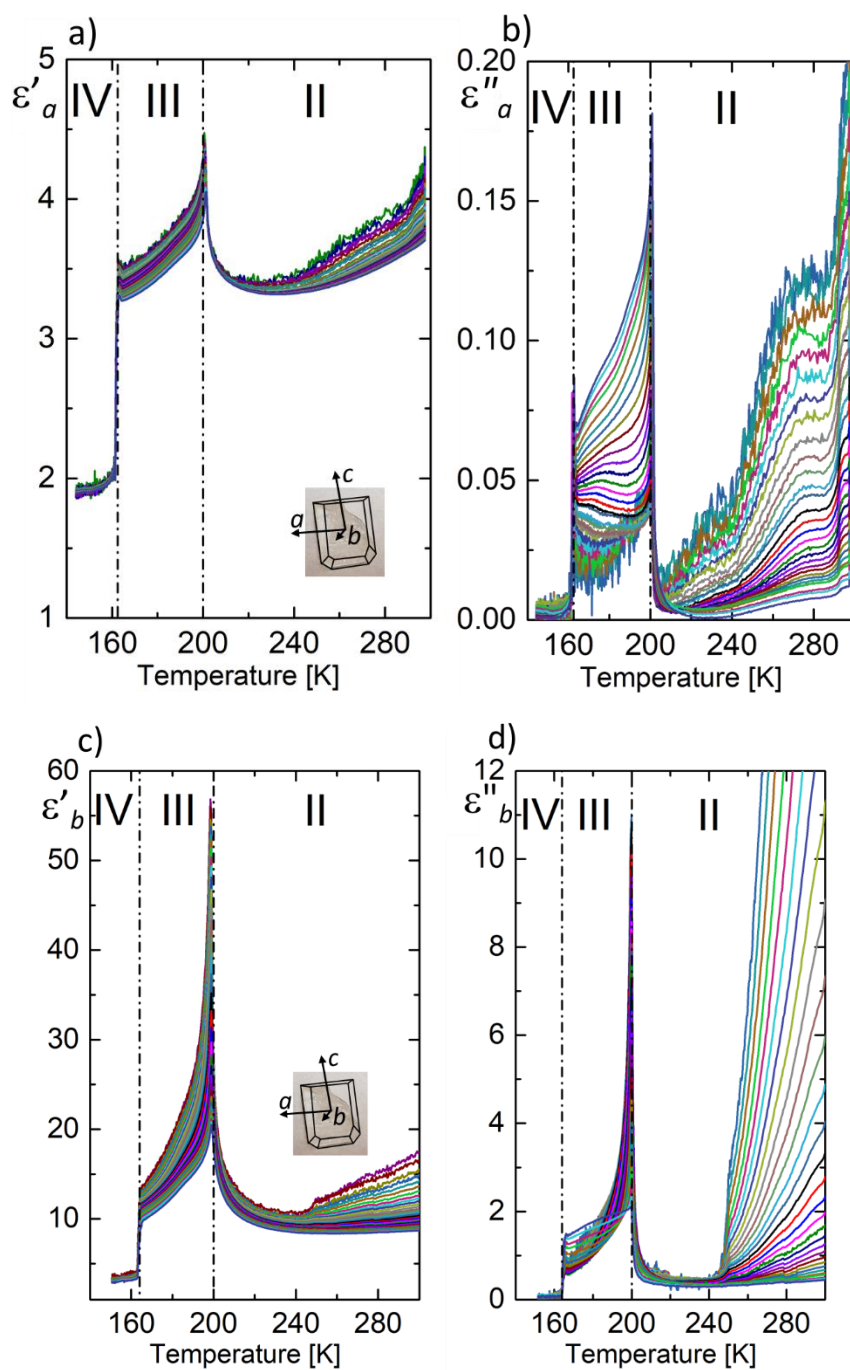


Figure S4. The temperature dependence of the dielectric permittivity, ε' and ε'' , obtained on cooling run for single crystals cut perpendicular to the a and b) a -axis ($S = 4 \text{ mm}^2$, $d = 1.1 \text{ mm}$), c and d) b -axis ($S = 16 \text{ mm}^2$, $d = 0.82 \text{ mm}$).

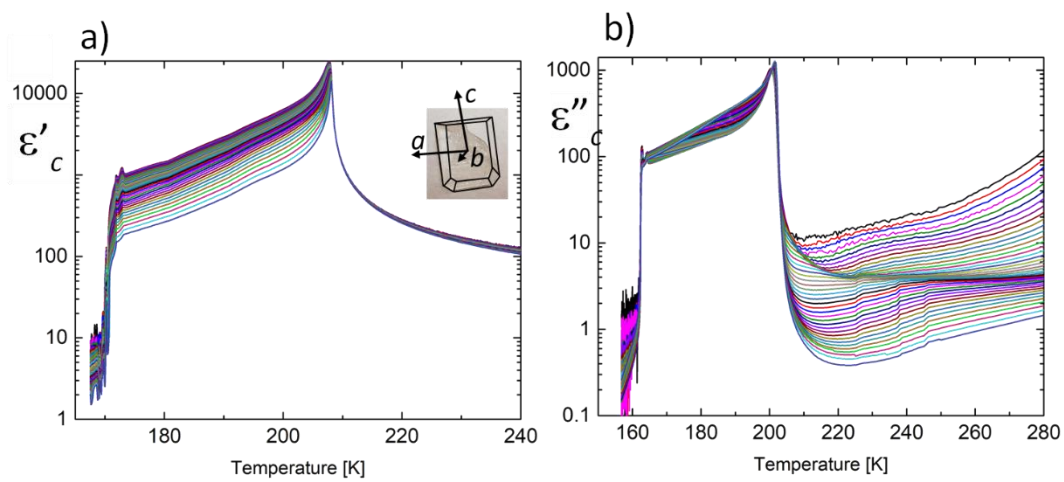


Figure S5. The temperature dependence of the dielectric permittivity, a) ϵ' and b) ϵ'' , obtained on cooling run for single crystals cut perpendicular to the c -axis. The 'y' is in *log*-scale.

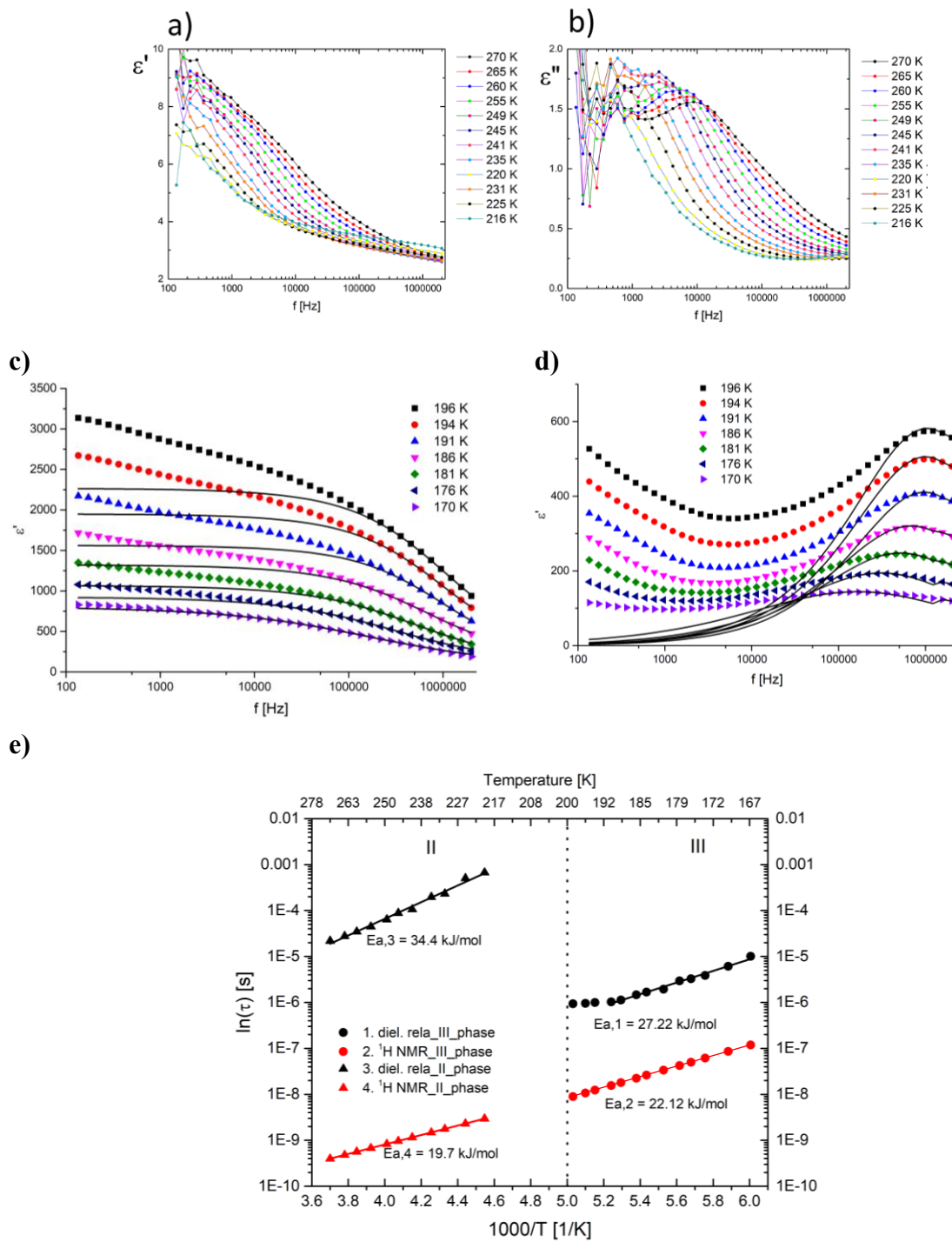


Figure S6. The frequency dependence of the dielectric permittivity, (a) ϵ' and (b) ϵ'' , obtained on cooling run for single crystals cut perpendicular to the c -axis. Data was presented for chosen temperatures from **II** phase. (c) and (d) Data was presented for chosen temperatures from **III** phase. e) The temperature dependence of the macroscopic dielectric relaxation time presented in Arrhenius relation. Red points present the relaxation time from NMR measurement, black from dielectric relaxation

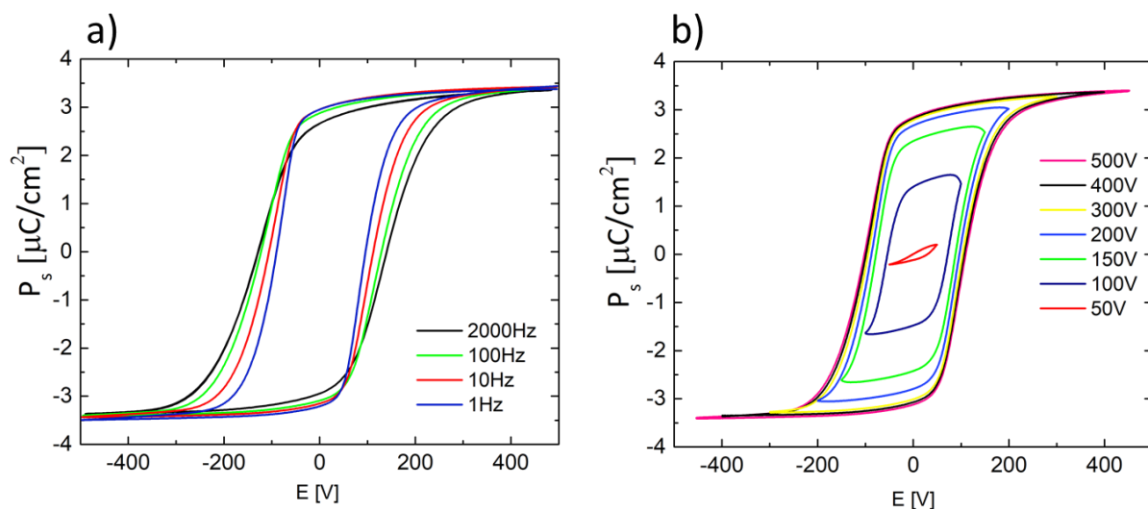


Figure S7. a) P-E vs. frequency and b) drive voltage for 1Hz. Both diagrams were measured at 170K.

Spontaneous polarization – theoretical calculations

The Berry phase calculations^{1,2} were performed for the ordered model of the non-centrosymmetric phase **III** (polar space group of $Cmc2_1$). The model was represented by two sets of coordinates, labelled with A and B, with azetidinium cations set manually to order the phase, in the way described later on. The atomic coordinates A and B are available in III_Cc_A.cif and III_Cc_B.cif files appended to Supplementary Materials. The reference crystal structure was measured at 185K.

Both LDA (Local Density Approximation, Teter Pade parametrization, keyword $ixc = 1$)³ and PBE (Perdew, Burke and Ernzerhof, $ixc = 11$) density functionals,⁴ as implemented in Abinit,^{5,6} were used against plane wave basis sets defined by the energy cut-off up to 500 eV.

The pseudopotentials used for these calculations were downloaded from <https://www.abinit.org>. In case of LDA calculations we used single projector, ordinary norm conserving pseudopotentials based on the Troullier-Martins method⁷, generated by D.C. Allan and A. Khein. For PBE calculations the pseudopotentials generated using FHI code were applied.

A dense Monkhorst–Pack k-point grid, i.e. $5 \times 2 \times 5$ ($\sim 0.03 \text{ \AA}^{-1}$) mesh in each direction in the Brillouin zone) was used for electronic structure calculations of the considered phase.⁸

Table S5. Spontaneous polarization components [$\mu\text{C}/\text{cm}^2$] for the ordered model of the non-centrosymmetric phase calculated within Berry phase approach using LDA functional. For ‘*a*’ axis a polarization indetermination quantum is a multiple of $14.90 \mu\text{C}/\text{cm}^2$. For ‘*c*’ axis a polarization indetermination quantum is a multiple of $13.37 \mu\text{C}/\text{cm}^2$.

energy cutoff [eV]	a	b	c
300	± 0.17	0.00	-3.13
400	± 0.16	0.00	-3.06
500	± 0.16	0.00	-3.05

Table S6. Spontaneous polarization components [$\mu\text{C}/\text{cm}^2$] for the ordered models of the non-centrosymmetric phase calculated within Berry phase approach using PBA functional.

energy cutoff [eV]	a	b	c
300	± 0.18	0.00	-3.07
400	± 0.17	0.00	-3.00
500	± 0.16	0.00	-2.98

The numerical data from Tables S5 and S6, representing the components of the spontaneous polarization of non-centrosymmetric phase **III**, show little dependence on the density functional selected for the electronic structure calculations and the cut-off energy.

For the ‘*a*’ component, for a given computational settings, two values are reported, which differ only by a sign. The negative value refers to the ordered model represented by A set of coordinates while the positive value originates in B set of coordinates.

A and B sets of coordinates differ in the position of atoms in CH_2 group containing C3 atom which in the original (disordered) phase may occupy one of the two positions equivalent due to $(-x, y, z)$ generator of $Cmc2_1$ space group (**Figure S8, Figure 4b** in the main body of the paper). Setting the position of the group (and consequently the positions of other disordered hydrogen atoms attached to C2 and C2’) removes the disorder and lowers the symmetry of the phase to Cc space group. Note, A and B are two sets of coordinates representing the same (ordered) structure.

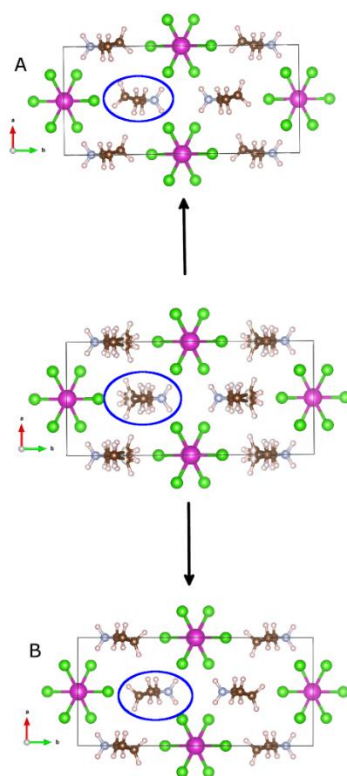


Figure S8. Graphical representation of the disordered phase **III** ($Cmc2_1$) and representations A and B of the ordered phase obtained by fixing the position of the azetidinium cation.

Within the assumed model, the spontaneous polarization of the disordered phase **III** can be obtained as an average over the polarizations calculated for the ordered structure represented by A and B. Hence, the only non-zero component of the spontaneous polarization is ‘ c ’ component whose value calculated using the largest basis set is in a narrow range of $(-3.05 - 2.98) \mu\text{C}/\text{cm}^2$ depending on the density functional applied for the calculations. Note, the sign of the component depends on the choice of the coordinate system to describe the atomic position and is physically meaningless.

A spontaneous polarization calculated using the Berry phase approach is always accompanied by the polarization indetermination quantum whose value results directly from the crystal cell parameters. Hence, the calculated numbers have to be interpreted against the experimental results. The apparent agreement between the value of the spontaneous polarization measured for phase **III** (about $4 \mu\text{C}/\text{cm}^2$ (168K), $3 \mu\text{C}/\text{cm}^2$ (179K), $2.5 \mu\text{C}/\text{cm}^2$ (187K), from polarization-electric hysteresis loop) and the basic values of ‘ c ’ component tabulated in S5 and S6 indicates that the basic values are of physical significance.

Interestingly, the ‘ a ’ component of the spontaneous polarization calculated for the ordered model derived from phase **III** is small, ca. 19 times smaller the ‘ c ’ component.

- (1) Vanderbilt, D.; King-Smith, R. D. Electric Polarization as a Bulk Quantity and Its Relation to Surface Charge. *Phys. Rev. B* **1993**, *48* (7), 4442–4455.
- (2) King-Smith, R. D.; Vanderbilt, D. Theory of Polarization of Crystalline Solids. *Phys. Rev. B* **1993**, *47* (3), 1651–1654.
- (3) Ceperley, D. M.; Alder, B. J. Ground State of the Electron Gas by a Stochastic Model. *Phys. Rev. Lett.* **1980**, *45* (7), 566–569.
- (4) Perdew, J.; Burke, K.; Ernzerhof, M. Generalized Gradient Approximation Made Simple. *Phys. Rev. Lett.* **1996**, *77* (18), 3865–3868.
- (5) Gonze, X.; Beuken, J. M.; Caracas, R.; Detraux, F.; Fuchs, M.; Rignanese, G. M.; Sindic, L.; Verstraete, M.; Zerah, G.; Jollet, F.; et al. First-Principles Computation of Material Properties: The ABINIT Software Project. *Comput. Mater. Sci.* **2002**, *25* (3), 478–492.
- (6) Gonze, X.; Jollet, F.; Abreu Araujo, F.; Adams, D.; Amadon, B.; Applencourt, T.; Audouze, C.; Beuken, J. M.; Bieder, J.; Bokhanchuk, A.; et al. Recent Developments in the ABINIT Software Package. *Comput. Phys. Commun.* **2016**, *205*, 106–131.
- (7) Troullier, N.; Martins, J. L. Efficient Pseudopotentials for Plane-Wave Calculations. II. Operators for Fast Iterative Diagonalization. *Phys. Rev. B* **1991**, *43* (11), 8861–8869.
- (8) Monkhorst, H. J.; Pack, J. D. Special Points for Brillouin-Zone Integrations. *Phys. Rev. B* **1976**, *13* (12), 5188–5192.

Figure S9 shows the second-moment values for protons of **AZECdCl₃** sample, where two distinct reduction of the Second moment M_2 are visible. The first reduction from about 24 G^2 to 12 G^2 occurs the phase transition 167K as expected with the fact that the puckering movement starts abruptly at this phase transition.⁹ The value of the dipolar second moment $M_2^{\text{Rigid}} = 17.1 G^2$ for a rigid azetidine molecule was calculated from the van Vleck formula¹⁰ with assumed distances C-H 1.09 Å and N-H 1.03 Å. The obtained theoretical M_2 value (an INTER contribution must be made to the total second moment M_2 resulting from interactions between cations is estimated to be about 1 G^2) is distinctly smaller than the measured one. Such discrepancy is presumably the result of neglecting the possible dipole–dipole interaction of protons with unpaired electrons or the necessity to adopt shorter distances, especially N-H bonds, than assumed for the calculations. For example, taking the N-H 0.89 Å distance into the calculations leads to a consistent result. However, there is also a surprisingly next second moment M_2 reduction from 12 G^2 to 8.7 G^2 at much higher temperatures around 305K. It should be assumed that the found last reduction of the second moment means the appearance of some axial movement of the azetidine cation instead of puckering motion. This reduction of the second moment of the NMR line is not related to any phase transition and is only a manifestation of a clear change in the dynamics of the azetidine cation in this temperature range

- (9) Asaji, T. Molecular Motion of Azetidinium Ion and Phase Transition in [(CH₂)₃NH₂]₂KCo(CN)₆ with Double Perovskite Structure. *Bull. Chem. Soc. Jpn.* **2021**, *94* (6), 1659–1663.
- (10) Van Vleck, J. H. The Dipolar Broadening of Magnetic Resonance Lines in Crystals. *Phys. Rev.* **1948**, *74*, 1168–1183.

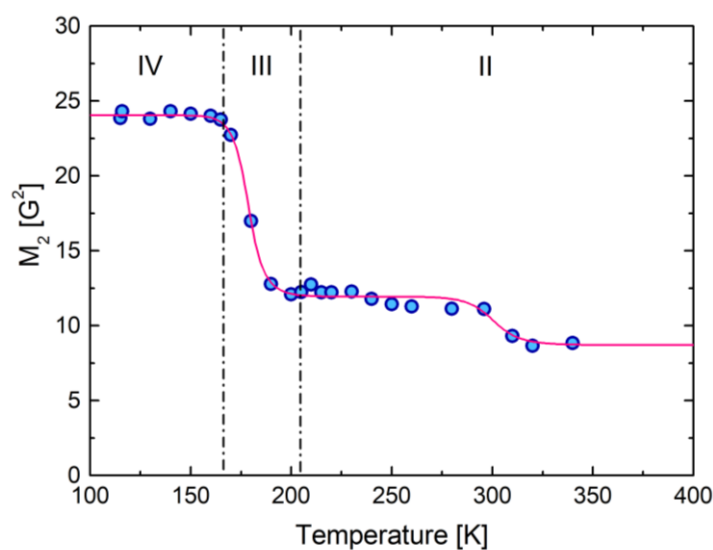


Figure S9. Temperature dependence of second moment of ¹H NMR line of **AZECdCl₃**.

Photoluminescence properties

Investigations on the optical properties of hybrid perovskites report that structural deformations of the inorganic lattice play the crucial role in the observed photoluminescence. This further suggests that distorted octahedral lattice of AZECdCl_3 may contribute to the electron-phonon coupling and favour to exciton self-trapping. Luminescence from such self-trapped excitons has been well studied in lead halides and alkali halides.^{11–15} Both peaks on excitation spectra (Figure S10) could be assigned to the excitons confined into the inorganic chain and could be attributed to the electronic transition from the 3p Cl orbitals in valence band to the 5s Cd level of the conduction band.

The temperature dependent emissions lifetime measurements were performed. All plotted profiles can be well fitted by two-exponential functions. As shown in Figure S14 and Table S7, as the temperature increases, the 370, 410 and 620 nm emissions lifetime decreases.

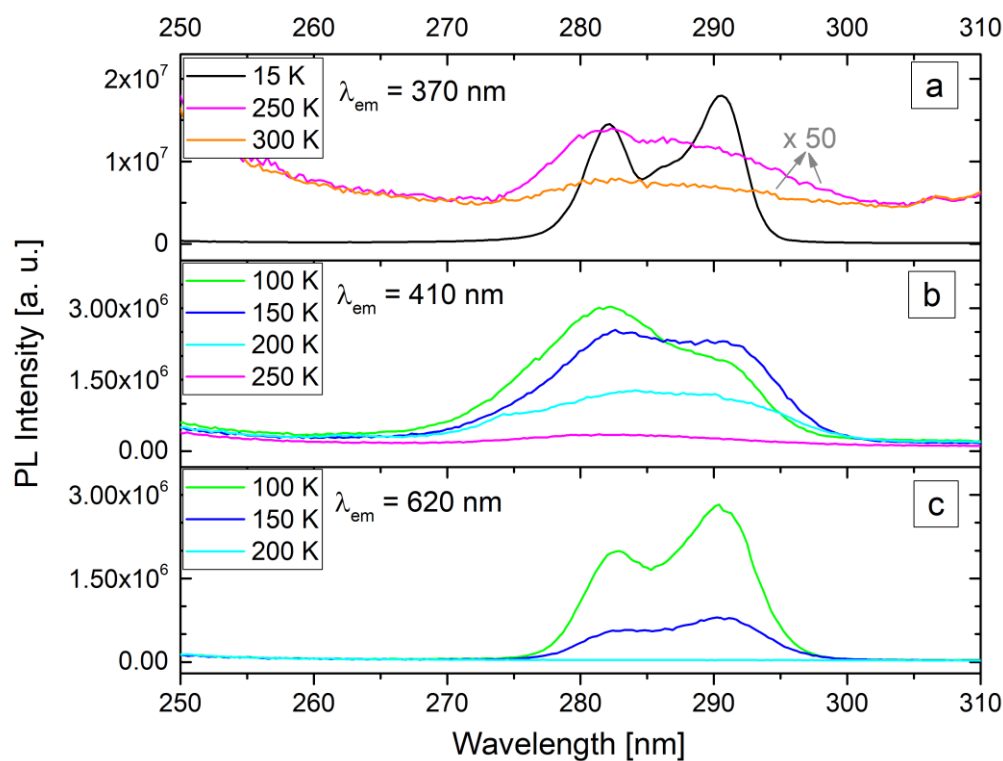


Figure S10. Temperature dependence of excitation spectra monitored at 370 nm (a), 410 nm (b) and 620 nm (c).

- (11) Yangui, A.; Garrot, D.; Lauret, J. S.; Lusson, A.; Bouchez, G.; Deleporte, E.; Pillet, S.; Bendeif, E. E.; Castro, M.; Triki, S.; et al. Optical Investigation of Broadband White-Light Emission in Self-Assembled Organic-Inorganic Perovskite (C₆H₁₁NH₃)₂PbBr₄. *J. Phys. Chem. C* **2015**, *119* (41), 23638–23647.
- (12) Iwanaga, M.; Hayashi, T. Exciton-Relaxation Dynamics in Lead Halides. *J. Lumin.* **2003**, *102–103* (SPEC), 663–668.
- (13) Iwanaga, M.; Shirai, M.; Tanaka, K.; Hayashi, T. Self-Trapped States and Related Luminescence in PbCl₂ Crystals. *Phys. Rev. B - Condens. Matter Mater. Phys.* **2002**, *66* (6), 643041–643048.
- (14) Wood, R. F. Luminescence from Exciton and Vk-Plus-Electron States in Alkali Halide Crystals. *Phys. Rev.* **1966**, *151*, 629–641.
- (15) Yuan, Z.; Zhou, C.; Tian, Y.; Shu, Y.; Messier, J.; Wang, J. C.; Van De Burgt, L. J.; Kountouriotis, K.; Xin, Y.; Holt, E.; et al. One-Dimensional Organic Lead Halide Perovskites with Efficient Bluish White-Light Emission. *Nat. Commun.* **2017**, *8*.

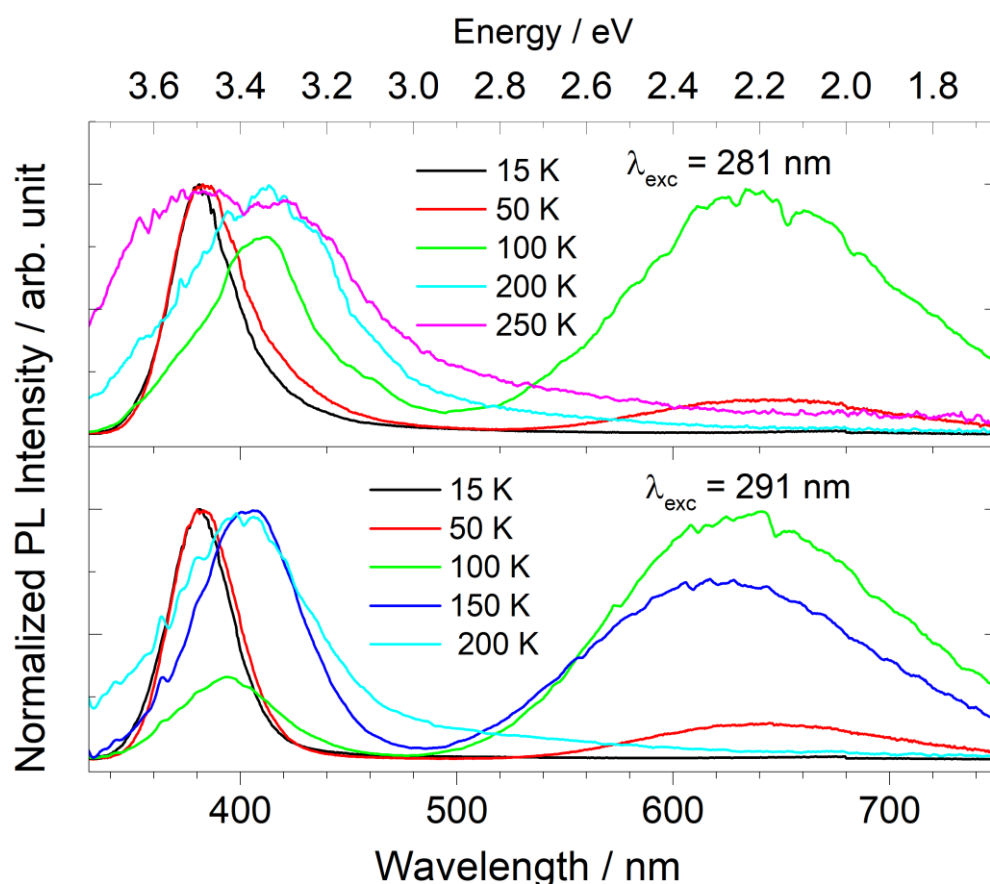


Figure S11. Normalized temperature-dependent emission spectra excited with (a) 281 nm and (b) 291 nm.

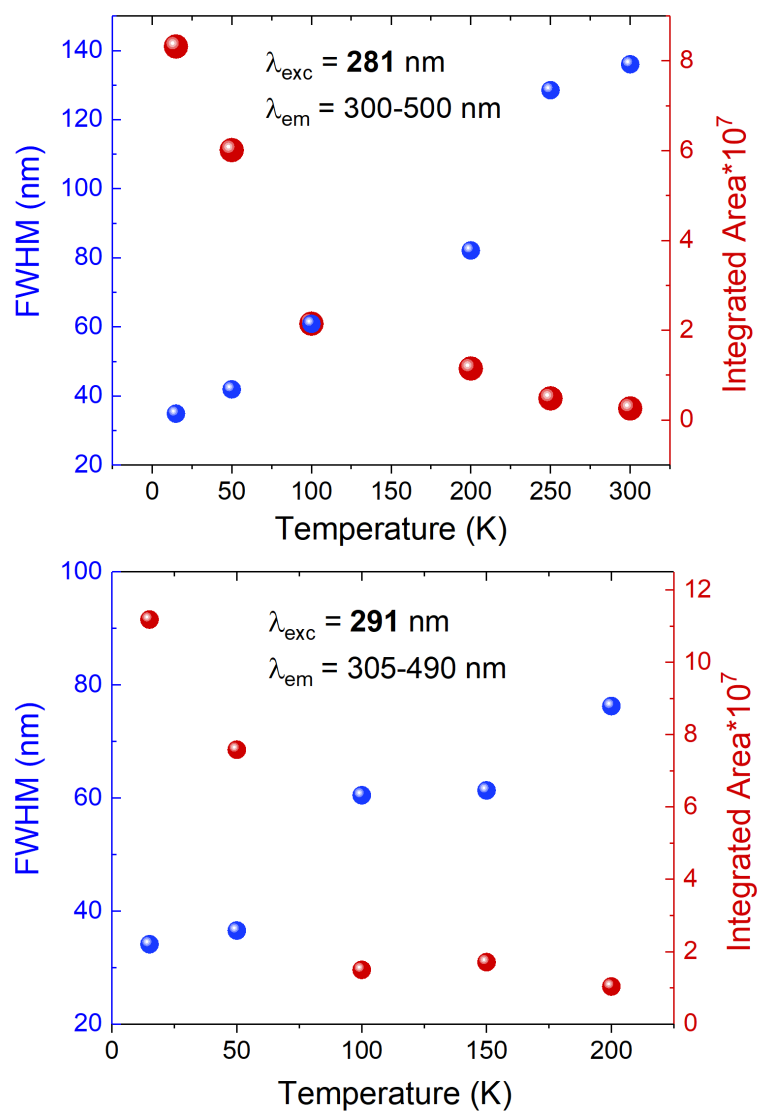


Figure S12. Temperature dependence of the integrated emission intensity (brown spheres) and FWHM (blue spheres) for emission excited with 281 nm (top) and 291 nm (bottom).

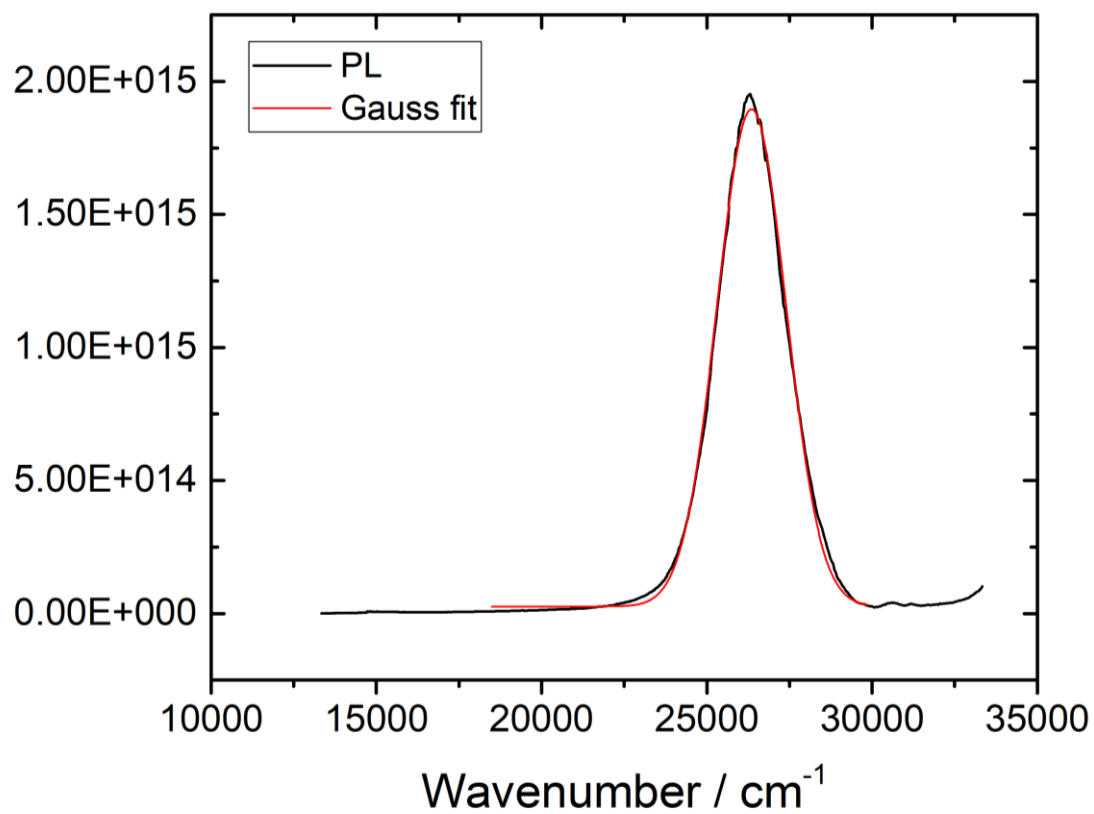


Figure S13. Gaussian deconvolution of 15K photoluminescence.

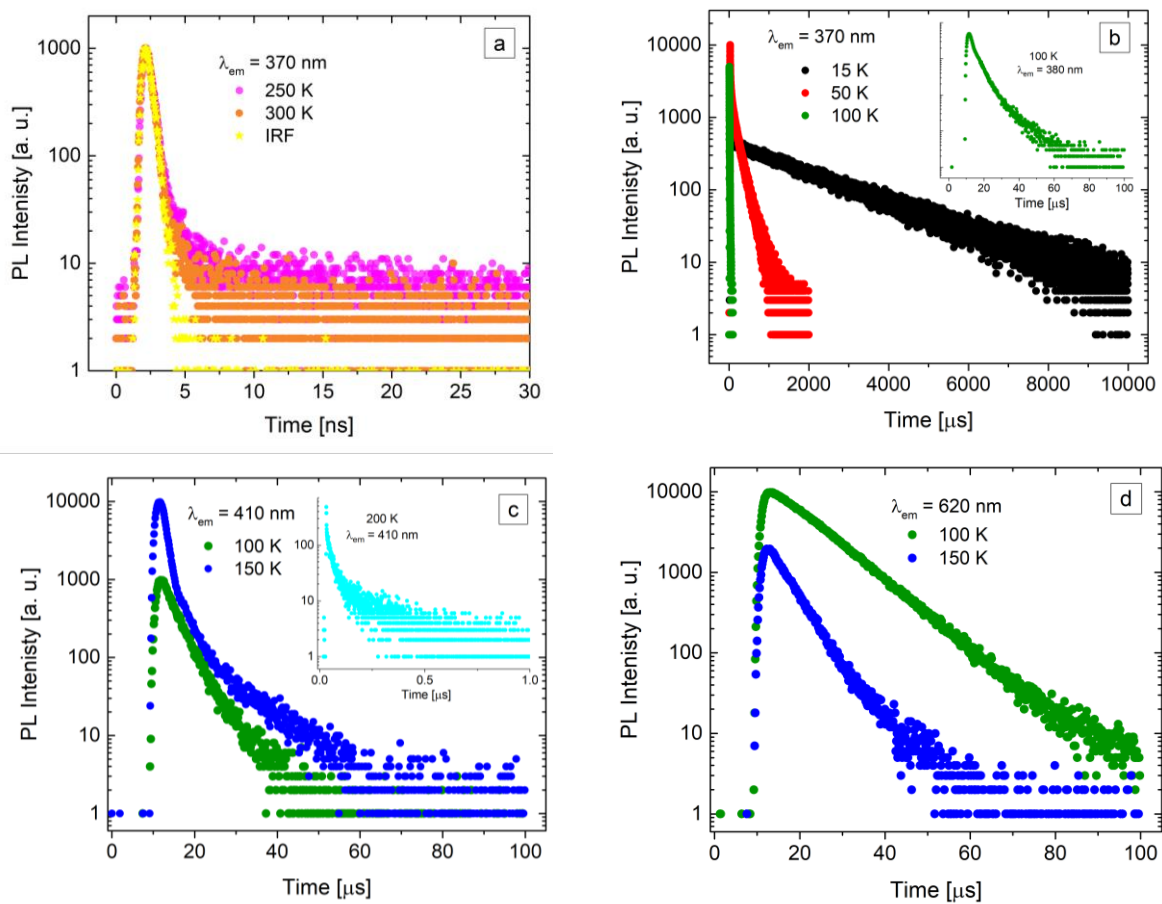


Figure S14. Temperature dependence of indicated emission decays.

Table S7. Temperature dependence of average lifetimes of indicated emissions.

Temperature [K]	τ_{av}		
	α_{em} : 370 nm	410 nm	620 nm
15	2.1 ms		
50	140 μ s		
100	5.1 μ s	4.1 μ s	9.2 μ s
150		830 ns	4.4 μ s
200		130 ns	
250	34.3 ns		
300	28.7 ns		

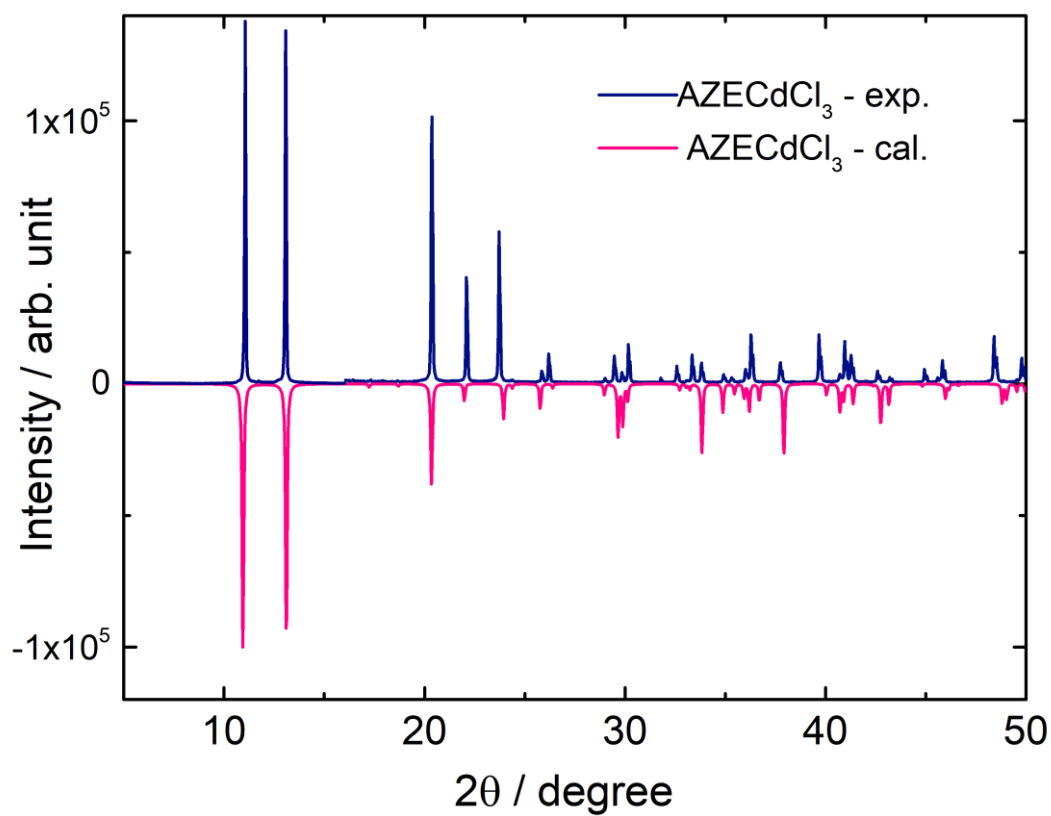


Figure S15. The X-ray diffraction pattern at 298 K of **AZECdCl₃** (blue) and calculated from crystal structure (pink).